RSC Advances

PAPER

View Article Online
View Journal | View Issue



Cite this: *RSC Adv.*, 2018, **8**, 25920

# Novel indole based hybrid oxadiazole scaffolds with *N*-(substituted-phenyl)butanamides: synthesis, lineweaver–burk plot evaluation and binding analysis of potent urease inhibitors†

Majid Nazir,[a] Muhammad Athar Abbasi, *[ab] Aziz-ur-Rehman,[a] Sabahat Zahra Siddiqui,[a] Hussain Raza,[b] Mubashir Hassan,[b] Syed Adnan Ali Shah,[c] Muhammad Shahid[d] and Sung-Yum Seo[b]

Received 11th June 2018
Accepted 5th July 2018

DOI: 10.1039/c8ra04987d

rsc.li/rsc-advances

In the study presented herein, 4-(1*H*-indol-3-yl)butanoic acid (**1**) was sequentially transformed in the first phase into ethyl 4-(1*H*-indol-3-yl)butanoate (**2**), 4-(1*H*-indol-3-yl)butanohydrazide (**3**) and 5-[3-(1*H*-indol-3-yl)propyl]-1,3,4-oxadiazole-2-thiol (**4**) as a nucleophile. In the second phase, various electrophiles were synthesized by reacting substituted-anilines, **5a–j**, with 4-chlorobutanoyl chloride (**6**) to afford 4-chloro-*N*-(substituted-phenyl)butanamides (**7a–j**). In the final phase, nucleophilic substitution reaction of **4** was carried out with different electrophiles, **7a–j**, to achieve novel indole based oxadiazole scaffolds with *N*-(substituted-phenyl) butamides (**8a–j**). The structural confirmation of all the as-synthesized compounds was performed by spectral and elemental analysis. These molecules were screened for their *in vitro* inhibitory potential against urease enzyme and were found to be potent inhibitors. The results of enzyme inhibitory kinetics showed that compound **8c** inhibited the enzyme competitively with a $K_i$ value 0.003 μM. The results of the *in silico* study of these scaffolds were in full agreement with the experimental data and the ligands showed good binding energy values. The hemolytic study revealed their mild cytotoxicity towards cell membranes and hence, these molecules can be regarded as valuable therapeutic agents in drug designing programs.



## 1. Introduction

Indole is an aromatic heterocyclic compound which exhibits a distinct reactivity. Indole is composed of a benzo-pyrrole in which the benzene and pyrrole rings are fused together through the 2- and 3-positions of the pyrrole ring. Indole can be deprotonated at the nitrogen end of the pyrrole ring. The salts thus formed prove to be good nucleophiles. The indole ring is found in many natural products such as fungal metabolites, indole alkaloids, and marine natural products. Highly ionic salts (*e.g.* $Li^+$, $K^+$) favor *N*-substitutions. Softer counter ions favor C-3 substitution.[1]

Indoles are found in various natural products and have been identified as compounds of chemical and biological importance. Indole is a highly conserved heterocyclic molecule that acts as a free radical scavenger and has a broad-spectrum of antioxidant activity. It has a unique place in biological systems, playing crucial roles in the form of amino acid, growth hormone and alkaloids. The indole core is also an important component in many recent drugs for treatment of chemotherapy-induced nausea and vomiting, cluster headache, or as antihypertensive, antineoplastic and antimitotic agents.[2–4] In addition, 1,3,4-oxadiazole derivatives have played a crucial part in theoretical development in heterocyclic chemistry and also used extensively in organic synthesis.[5,6] Considerable attention has been focused on 2,5-disubstituted-1,3,4-oxadiazole containing compounds due to their remarkable biological activity and also their importance in the pharmaceutical field. These compounds are effectively being utilized as antibacterials. Some of these compounds have also been recognized as anticancer, anti-Parkinson, anti-HIV and anti-proliferative agents as well.[7–9]

Urease belongs to a family of highly conserved urea-hydrolyzing enzymes. Urease is known to be one of the major causes of disease induced by *Helicobacter pylori*, thus allowing them to survive at low pH of the stomach and therefore, play an important role in the pathogenesis of gastric and peptic ulcer. *Proteus mirabilis* and *Yersinia enterocolitica* are responsible for urolithiasis and are involved in the development of acute pyelonephritis and infection-induced reactive arthritis,

[a]*Department of Chemistry, Government College University, Lahore-54000, Pakistan. E-mail: abbasi@gcu.edu.pk; Tel: +92-42-111000010 ext. 266*

[b]*College of Natural Science, Department of Biological Sciences, Kongju National University, Gongju, 32588, South Korea*

[c]*Faculty of Pharmacy, Atta-ur-Rahman Institute for Natural Products Discovery (AuRIns), Universiti Teknologi MARA, Level 9, FF3, Puncak Alam Campus, 42300 Bandar Puncak Alam, Selangor Darul Ehsan, Malaysia*

[d]*Department of Biochemistry, University of Agriculture, Faisalabad-38040, Pakistan*

† Electronic supplementary information (ESI) available. See DOI: 10.1039/c8ra04987d

respectively. The typical remedy for treating bacterial infection with antimicrobials has often proven futile, and only a few combination regiments have reached clinical practice. Thus, the need for alternative or novel treatments is evident.[10,11]

The bioactivity of indole and oxadiazole moieties prompted us to synthesize some new butanamide molecules bearing these moieties altogether. Hence, in continuation of our previous efforts on bioactivity study of indole containing compounds[12,13] and urease inhibitory activity of bi-heterocyclic bi-amide molecules,[14] the present investigation was designed to explore the urease inhibitory potential and the kinetic mechanism of newly synthesized bi-heterocyclic butanamides. The binding interactions with the targeted enzyme were ascertained by molecular docking, and the cytotoxicity of these scaffolds was evaluated by hemolysis to identify their therapeutic utility as promising drug candidates in drug discovery programs.

## 2. Materials and methods

### 2.1 General

All the chemicals, along with analytical grade solvents, were purchased from Sigma Aldrich, Alfa Aesar (Germany), or Merck, through local suppliers. Pre-coated silica gel Al-plates were used for TLC with ethyl acetate and *n*-hexane as solvent systems. Spots were detected by $UV_{254}$. Gallonkamp apparatus was used to detect melting points in capillary tubes. Infrared (IR) spectra ($\nu$, $cm^{-1}$) were recorded by the pellet method using a Jasco-320-A spectrophotometer. Elemental analyses were performed on a Foss Heraeus CHN-O-Rapid instrument and were within $\pm$0.4% of the theoretical values. Electron Impact Mass Spectrometry (EI-MS) spectra were measured on a JEOL JMS-600H instrument with a data processing system. Proton Nuclear Magnetic Resonance ($^1$H-NMR) spectra ($\delta$, ppm) were recorded at 600 MHz [Carbon Nuclear Magnetic Resonance ($^{13}$C-NMR) spectra, at 150 MHz] in DMSO-$d_6$ using a Bruker Advance III 600 Ascend spectrometer with a BBO probe. The $^1$H-NMR spectral peaks for interpretation are abbreviated as follows: s, singlet; d, doublet; dd, doublet of doublets; t, triplet; br.t, broad triplet; q, quartet; quint, quintet; sex, sextet; sep, septet; m, multiplet, dist, distorted. The structural characterization of all compounds is given in the ESI.†

### 2.2 Synthesis of ethyl 4-(1*H*-indol-3-yl)butanoate (2)

4-(1*H*-indol-3-yl)butanoic acid (0.2 mol; **1**) dissolved in absolute ethanol (70 mL) and a catalytic amount of concentrated sulfuric acid (20 mL) were placed in a 500 mL round bottom (RB) flask and refluxed for 8 h until the maximum completion of reaction, as determined through TLC. At the end, the reaction mixture was neutralized with 10% aqueous sodium carbonate (40 mL). The product was isolated by solvent extraction with chloroform (50 mL $\times$ 3). The solvent was distilled off and the required ester, **2**, was obtained as a reddish brown liquid.

### 2.3 Synthesis of 4-(1*H*-indol-3-yl)butanohydrazide (3)

4-(1*H*-indol-3-yl)butanoate (0.15 mol.; **2**) in 60 mL methanol and hydrazine monohydrate (80%; 25 mL) were placed in a 500 mL round bottom flask. The reaction mixture was stirred for 14 h at room temperature (RT). After absolute conversion, the acid hydrazide was obtained by distilling methanol off from the reaction mixture. The precipitates were filtered, washed with cold *n*-hexane and air-dried to get pure 4-(1*H*-indol-3-yl) butanohydrazide (**3**).

### 2.4 Synthesis of 5-[3-(1*H*-indol-3-yl)propyl]-1,3,4-oxadiazole-2-thiol (4)

4-(1*H*-indol-3-yl)butanohydrazide (0.13 mol; **3**) in absolute ethanol (30 mL) and KOH (0.13 mol) were placed in a round bottom flask. Carbon disulfide (0.26 mol) was added subsequently. The mixture was refluxed for 16 h. On completion of the reaction, excess chilled distilled water and dil. HCl was added to adjust to pH 5–6. The precipitates were filtered, washed and dried to get the desired cyclized product, **4**.

### 2.5 Preparation of 4-chloro-*N*-(un/substituted-phenyl) butanamides (7a–j)

Synthesis of various 4-chloro-*N*-(un/substituted-phenyl) butanamides (**7a–j**) was carried out by reaction of various aryl amines (**5a–j**) with 4-chlorobutanoyl chloride (**6**) in equimolar quantities (0.001 moles) and shaking manually in 10% aqueous $Na_2CO_3$ solution. Solid precipitates were formed after 20–30 min, and then filtered and washed with cold distilled water to obtain the desired electrophiles, **7a–j**.

### 2.6 Synthesis of 4-({5-[3-(1*H*-indol-3-yl)propyl]-1,3,4-oxadiazol-2-yl}sulfanyl)-*N*-(substituted-phenyl)butanamides (8a–j)

5-[3-(1*H*-indol-3-yl)propyl]-1,3,4-oxadiazole-2-thiol (0.2 g, **4**) was added in DMF (5 mL) contained in a 250 mL round bottom flask at room temperature, and a small amount of LiH was added, followed by stirring for 30 min. Then, different 4-chloro-*N*-(substituted-phenyl)butanamides (**7a–j**) were added separately in equimolar amounts to each respective reaction mixture and stirred for 60–70 hours. The completion of the reaction was monitored by TLC; after completion, the reaction mixture was quenched with ice cold water (100 mL). The respective derivatives, **8a–j**, were collected through filtration or solvent extraction based on the nature of the product.

### 2.7 *In vitro* urease inhibitory activity

The Jack bean urease activity was determined by measuring the amount of ammonia produced *via* the indophenols method, as reported.[15,16] The reaction mixtures, comprised of 20 μL of enzyme (Jack bean urease, 5 U/mL) and 20 μL of compounds in 50 μL potassium phosphate buffer (100 mM urea, 10 mM $K_2HPO_4$, 1 mM EDTA and 10 mM LiCl, pH 8.2), were incubated for 30 min at 37 °C in 96-well plate. Briefly, 50 μL each of the phenol reagents (1%, w/v phenol and 0.005%, w/v sodium nitroprusside) and 50 μL of the alkali reagent (0.5%, w/v NaOH and 0.1% sodium hypochlorite NaOCl) were added to each well. The absorbance at 625 nm was measured after 10 min, using a microplate reader ($OPTI_{Max}$, Tunable). All the reactions were

performed in triplicate. The urease inhibition activities were calculated according to the following formula:

$$\text{Urease inhibition activity (\%)} = (\text{OD}_{\text{control}} - \text{OD}_{\text{sample}} \times 100)/\text{OD}_{\text{control}} \quad (1)$$

where $\text{OD}_{\text{control}}$ and $\text{OD}_{\text{sample}}$ represents the optical densities in the absence and presence of sample, respectively. Thiourea was used as the positive control for the urease activity.

### 2.8 Kinetic analysis

Kinetic analysis was carried out to determine the mode of inhibition. Compound **8c** was selected on the basis of the lowest $IC_{50}$ value. The kinetics was carried out by varying the concentration of urea in the presence of different concentrations of **8c** (0.00, 0.017, and 0.034 μM). Briefly the urea concentration was changed from 100, 50, 25, 12.5 and 6.25 mM for the urease kinetics studies and the remaining procedure was the same for all kinetic studies, as described in the urease inhibition assay protocol. Maximal initial velocities were determined from the initial linear portion of absorbance up to 10 minutes after addition of the enzyme at per-minute intervals. The mode of inhibition of the enzyme was assayed *via* the Lineweaver–Burk plot of the inverse of the velocities ($1/V$) *versus* the inverse of the substrate concentration $1/[S]$ $mM^{-1}$. The EI dissociation constant, $K_i$, was determined by secondary plot of $1/V$ *versus* the inhibitor concentration. The urease activity was determined by measuring ammonia production using the indophenol method, as reported previously.[17,18] The results (change in absorbance per min) were processed by using the SoftMaxPro software.

### 2.9 Computational methodology

**2.9.1 Retrieval of Jack bean urease from Protein Data Bank.** The jack bean urease structure (*C. ensiformis*) at 1.52 resolution was obtained from the Protein Data Bank (PDB) having PDBID 4H9M (https://www.rcsb.org/structure/4h9m). The accessed receptor molecule was further minimized by employing UCSF Chimera 1.10.1 tool.[19] The Ramachandran plot and values were accessed from the PDB. The protein architecture and statistical percentage values of the receptor proteins, α-helices, β-sheets, coils and turns were predicted from the online server, VADAR 1.8.[20]

**2.9.2 Molecular docking simulation.** Before docking the experiment, all the synthesized chemical structures were sketched in ACD/ChemSketch tool and accessed in mol format. Furthermore, the UCSF Chimera 1.10.1 tool was employed for energy minimization of each ligand, separately, having default parameters as follows: steepest descent steps, 100 with step size of 0.02 (Å); conjugate gradient steps, 100 with step size 0.02 (Å); and update interval: 10. Finally, Gasteiger charges were added using Dock Prep in the ligand structure to obtain good structure conformation. Molecular docking experiment was employed on all the ligands, **8a–j**, against Jack bean urease by using virtual screening too PyRx with the VINA Wizard approach.[21] The values of the grid box parameters in the VINA search space ($X = 10.22$, $Y = 24.56$ and $Z = 46.18$) were adjusted with default exhaustiveness value = 8 to maximize the binding conformational analysis. We adjusted the grid box size on biding pocket residues to sufficiently allow the ligand to move freely in the search space. All the as-synthesized ligands were docked separately against the target protein. In all of the docked complexes, the conformational poses of ligand were keenly observed to obtain the best docking results. The generated docked complexes were evaluated on the basis of the lowest binding energy (kcal $mol^{-1}$) values and structure activity relationship (SAR) analyses. The three dimensional (3D) graphical depictions of all the docked complexes were accomplished by using the UCSF Chimera 1.10.1 and Discovery Studio (2.1.0) programs.[22]

### 2.10 Hemolytic activity

Bovine blood sample was collected in EDTA, which was diluted with saline (0.9% NaCl), and centrifuge at 1000 × *g* for 10 min. Erythrocytes were separated and diluted in phosphate buffer saline (PBS) of pH 7.4 and a suspension was made. The test compound solution (20 μL, 10 mg $mL^{-1}$) was mixed with 180 μL of RBCs suspension and incubated for 30 min at room temperature. PBS was used as a negative control and Triton 100-X was taken as a positive control.[23,24] The experiments were carried out with the control in triplicate. Statistical analysis was performed by Microsoft Excel 2010 for all the measurements and the results are presented as mean ± SEM. The % age of hemolysis was obtained by using the formula:

$$(\%)\ \text{of hemolysis} = \frac{\text{Absorbance of sample} - \text{Absorbance of negative control}}{\text{Absorbance of positive control}} \times 100 \quad (2)$$

## 3. Results and discussion

### 3.1 Chemistry

The convergent syntheses of the targeted bi-heterocyclic butamide derivatives was accomplished in superb yields through several steps in three phases of reactions. In the first phase, 4-(1*H*-indol-3-yl)butanoic acid (**1**) was subjected to esterification by ethanol in the presence of concentrated sulfuric acid taken in a catalytic amount. Ethanol was used as reactant and also as a solvent in order to push the equilibrium towards the product, as it was a reversible reaction. The product was collected by solvent extraction after the addition of a weak base and excess water. The base was added to neutralize the catalytic sulfuric acid and the unreacted carboxylic acid. The salts of these acids were transferred to the aqueous layer, while the resultant ester was present in the organic phase during solvent extraction. Thus, ethyl 4-(1*H*-indol-3-yl)butanoate (**2**) was obtained as a brownish liquid (solid at refrigeration). The second step was performed to convert the ethyl ester to the respective carbohydrazide, **3**, by the nucleophilic hydrazine in the presence of an organic solvent such as methanol, and the mixture was set to

 

reflux for 14 hours. Thus, 4-(1*H*-indol-3-yl)butanohydrazide (**3**) was obtained as a light brown coloured solid. The third step was a cyclization to form a heterocyclic ring through reaction with $CS_2$ in a basic alcoholic medium. The resulting product was 5-[3-(1*H*-indol-3-yl)propyl]-1,3,4-oxadiazole-2-thiol (**4**), which had a mercapto group at its second carbon. In the second phase, different electrophiles were synthesized by reacting substituted-anilines (**5a–j**) with 4-chlorobutanoyl chloride (**6**) to afford 4-chloro-*N*-(substituted-phenyl)butanamides (**7a–j**). In the final phase, the acidic proton of **4** was replaced with the aforementioned electrophiles, **7a–j**, in the presence of LiH using aprotic polar medium to obtain the required molecules, **8a–j**, as sketched in Scheme 1 and structures of different derivatives have been drawn in Fig. 1.

The structural analysis of one of the compounds is discussed here in detail for the articulacy of the reader. The molecule **8g** was obtained as a brown sticky liquid. Its molecular formula, $C_{25}H_{28}N_4SO_2$, was established by CHN analysis data and its molecular ion peak in its EI-MS spectrum (*m*/*z* 448 (Fig. 2)). The number of proton and carbon resonances in its $^1$H-NMR and $^{13}$C-NMR spectra were also in agreement with its deduced molecular formula. Different functionalities in this molecule were depicted by absorption bands in its IR spectrum at $\nu$ 3226 (N–H str.), 2942 (C–H str. of aromatic ring), 1673 (C=O str.), 1648 (C=N Str.), 1585 (C=C aromatic str.), 1520, 1477, 1415 (Str. for oxadiazole), 1159 (C–O–C Str.), 644 (C–S str.) cm$^{-1}$.

With the help of $^1$H-NMR spectrum of this molecule, the indole heterocyclic core was identified clearly by the characteristic signals at $\delta$ 10.80 (s, 1H, NH-1), 7.51 (br.d, $J$ = 7.8 Hz, 1H, H-7), 7.34 (br.d, $J$ = 8.1 Hz, 1H, H-4), 7.14 (dist.d, $J$ = 1.8 Hz, 1H, H-2), 7.06 (br.t, $J$ = 7.2 Hz, 1H, H-6) and 6.97 (br.t, $J$ = 7.2 Hz, 1H, H-5) ppm.[12] Similarly, the resonances at $\delta$ 7.21 (br.d, $J$ = 7.9 Hz, 1H, H-6‴′), 7.00 (br.s, 1H, H-3‴′), 6.94 (br.d, $J$ = 7.7 Hz, 1H, H-5‴′), along with two methyl signals at $\delta$ 2.23 (s, 3H, $CH_3$-4‴′) and 2.12 (s, 3H, $CH_3$-2‴′) ppm, were typical for a 2,4-dimethylphenyl group in the molecule. The C and *N*-substituted butanamide group was identified by four signals at $\delta$ 9.25 (s, 1H, CONH-1), 3.27 (t, $J$ = 7.1 Hz, 2H, $CH_2$-4‴), 2.47 (t, $J$ = 7.2 Hz, 2H, $CH_2$-2‴) and 2.06–2.01 (m, 4H, $CH_2$-3‴ & $CH_2$-2′). In the up-field region of the spectrum, the signals of three intervening methylene groups at $\delta$ 2.87 (t, $J$ = 7.4 Hz, 2H, $CH_2$-3′), 2.77 (t, $J$ = 7.3 Hz, 2H, $CH_2$-1′), and 2.06–2.01 (m, 4H, $CH_2$-3‴ & $CH_2$-2′), were helpful in ascertaining the connectivity of the indole moiety from its 3-position to the 5-position of the 1,3,4-oxadiazole scaffold. The $^1$H-NMR spectrum of this compound is shown in Fig. 3(a, b and c).

The carbon skeleton of this molecule was also fully corroborated by its $^{13}$C-NMR spectrum, shown in the Fig. 4. The signals in its $^{13}$C-NMR spectrum were rational for all the twenty five carbons, where the most downfield quaternary carbons signals at $\delta$ 168.32 (C-5″) and 163.36 (C-2″) belonged to the cyclized 1,3,4-oxadiazole ring, thus confirming the formation of

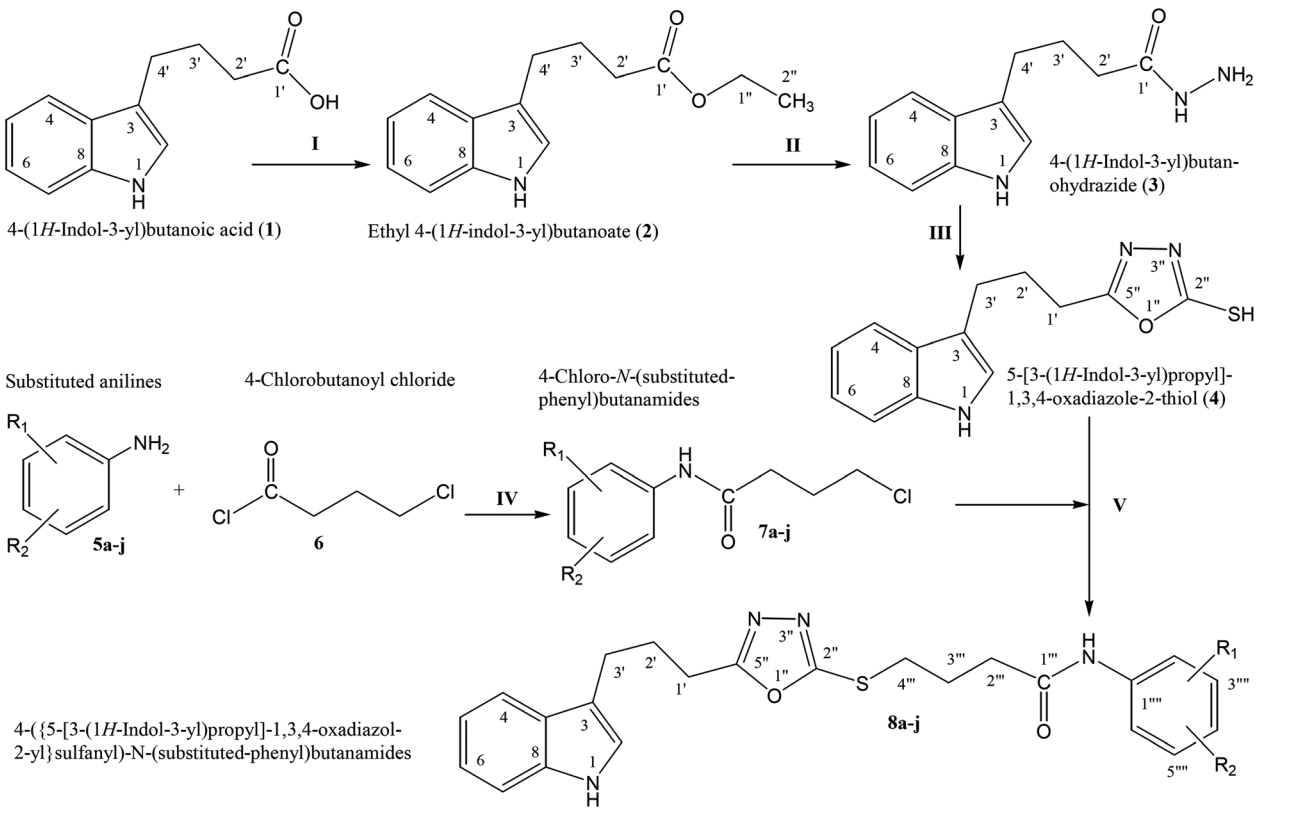


Scheme 1 Outline for the synthesis of 4-({5-[3-(1*H*-indol-3-yl)propyl]-1,3,4-oxadiazol-2-yl}sulfanyl)-*N*-(substituted-phenyl)butanamides (**8a–j**). For $-R_1$ and $-R_2$, see structures of derivatives (Fig. 1). Reagents & conditions: (I) EtOH/$H_2SO_4$/refluxing for 8 h (II) MeOH/$N_2H_4 \cdot H_2O$/refluxing for 14 h (III) EtOH/$CS_2$/KOH/refluxing for 16 h (IV) Aq. $Na_2CO_3$ soln/pH 9–10/vigorous shaking at RT for 20–30 minutes. (V) DMF/LiH/stirring for 60–70 h.

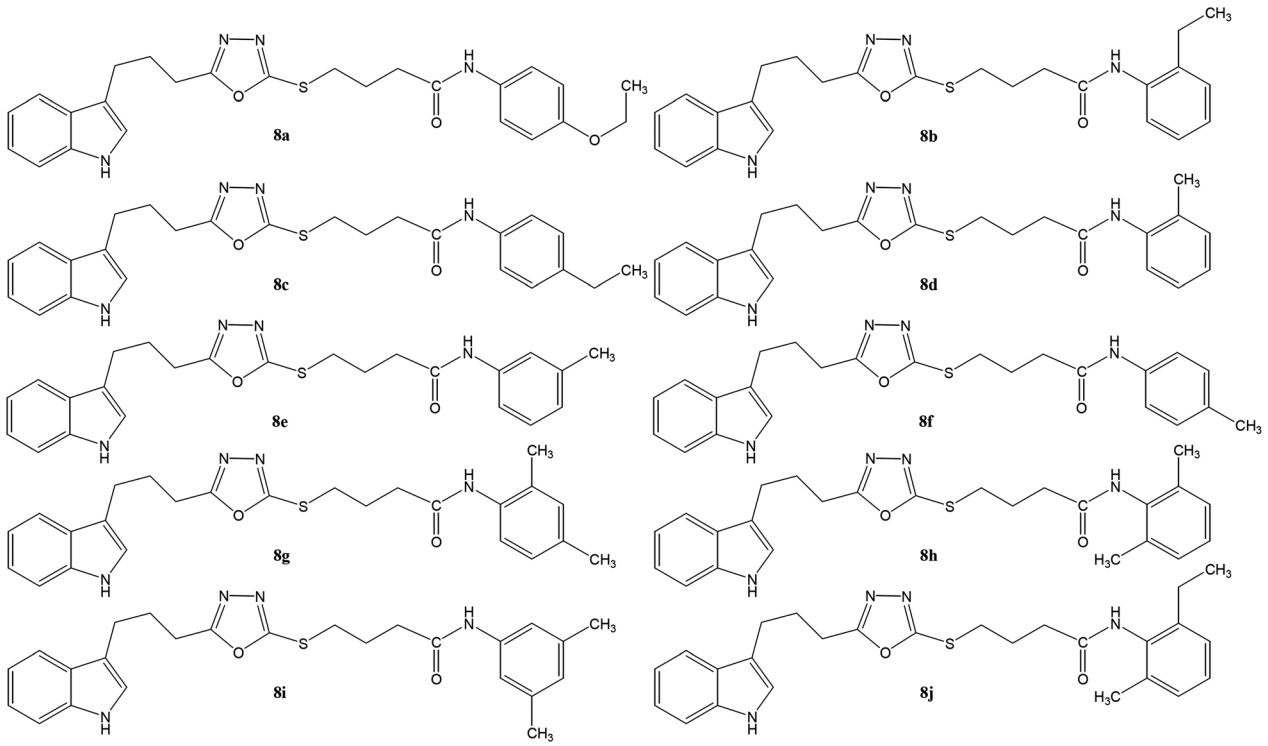


Fig. 1 Structures of different derivatives, **8a–j**.

this heterocyclic core. The other three quaternary carbons appearing at $\delta$ 136.79 (C-8), 127.50 (C-9), and 113.78 (C-3) ppm, were attributed to the indole moiety. The methine carbon resonances appearing at $\delta$ 122.97 (C-2), 121.35 (C-6), 118.66 (C-5 & 7), 111.83 (C-4) were also coherent with the indole moiety.[13] The C and *N*-substituted butanamido group was confirmed by

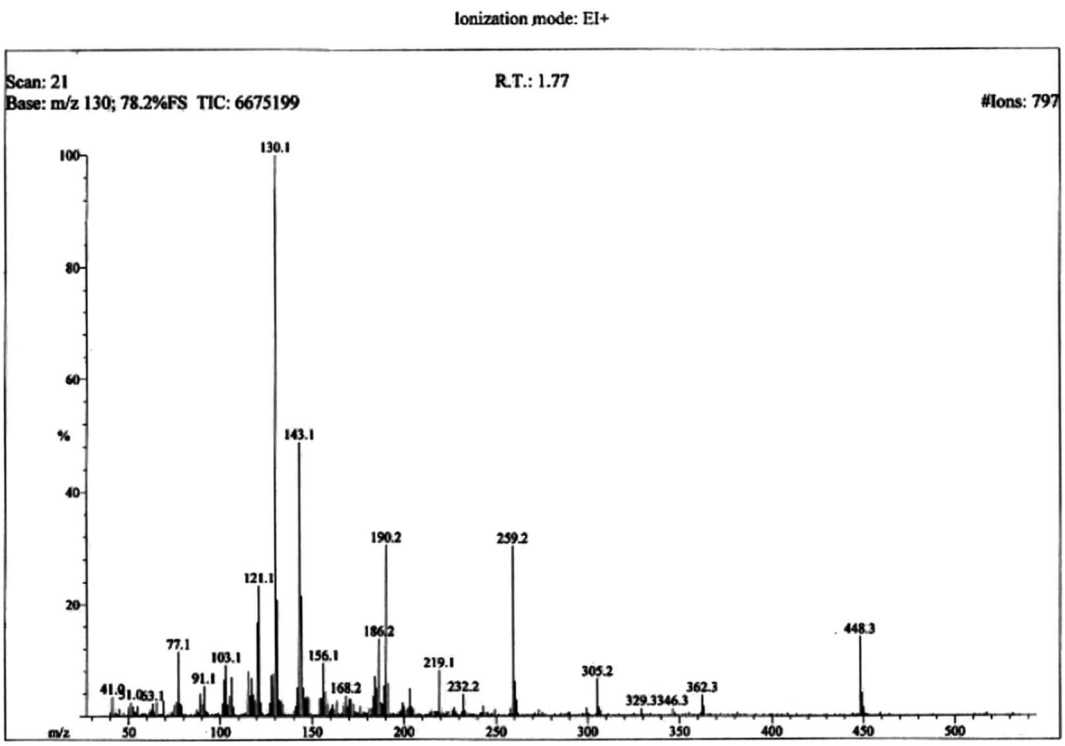


Fig. 2 EI-MS spectrum of **8g**.

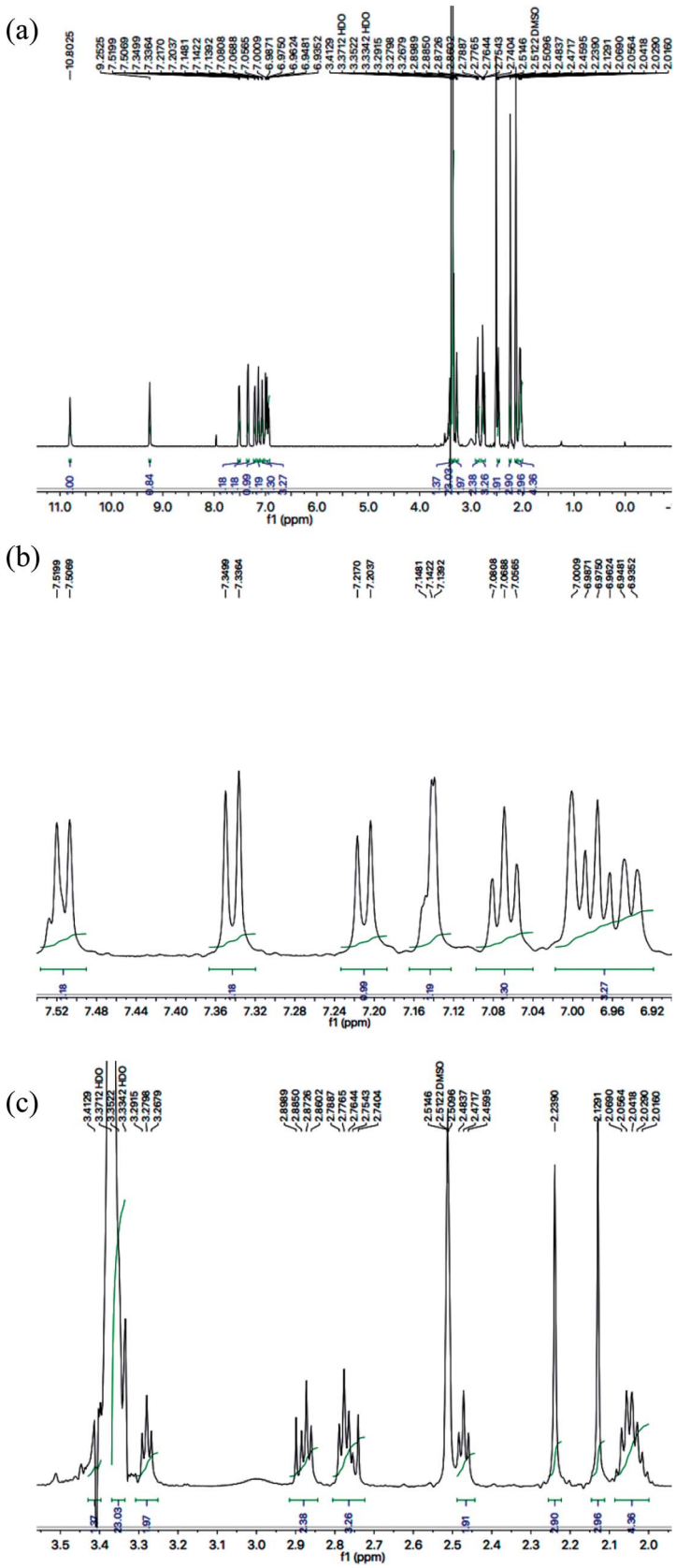


Fig. 3 (a) $^{1}$H-NMR spectrum of **8g**. (b) Expanded aromatic region of $^{1}$H-NMR spectrum of **8g**. (c) Expanded aliphatic region of $^{1}$H-NMR spectrum of **8g**.

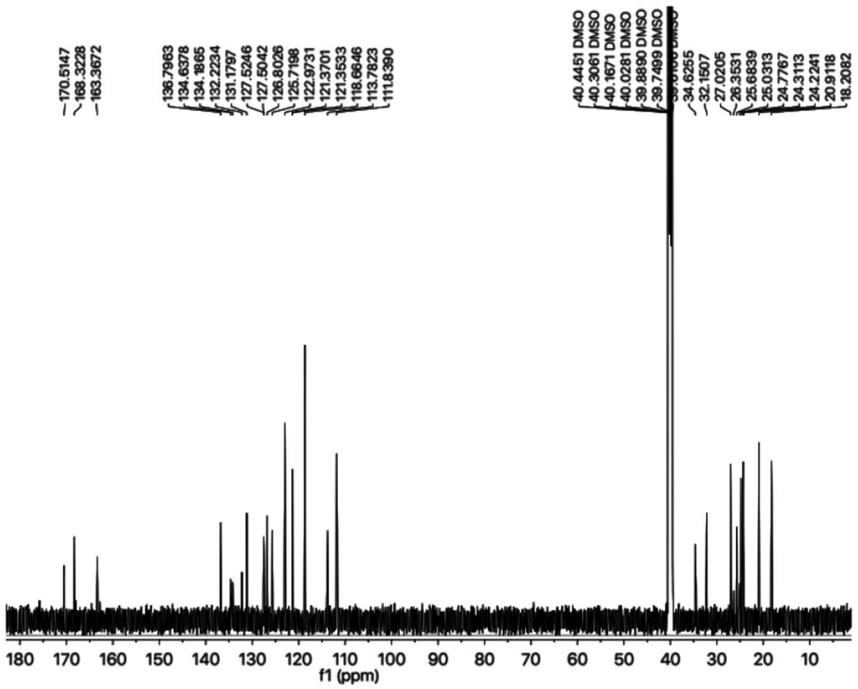


Fig. 4 $^{13}$C-NMR spectrum of **8g** molecule.

two discrete resonances, one for a carbonyl group at $\delta$ 170.51 (C-1‴) and other for three methylene groups at $\delta$ 34.62 (C-2‴), 32.15 (C-4‴) and 25.68 (C-2‴). The 2,4-dimethylphenyl group attached to a nitrogen atom was thoroughly substantiated by three quaternary signals at $\delta$ 134.63 (C-1⁗), 134.18 (C-2⁗) and 132.22 (C-4⁗), three methine signals at $\delta$ 131.17 (C-5⁗), 126.80 (C-3⁗) and 125.71 (C-6⁗), and two methyl signals at $\delta$ 20.91 ($CH_3$-4⁗) and 18.20 ($CH_3$-2⁗). In the up-field region of the spectrum, three signals at $\delta$ 27.02 (C-1′), 24.77 (C-3′), and 24.31 (C-2′) were characteristic for three connected methylenes, which adjoined the indole moiety with the heterocyclic oxadiazole core in the molecule. So, on the basis of the aforesaid cumulative evidences, the structure of **8g** was confirmed and it was named *N*-(2,4-dimethylphenyl)-4-({5-[3-(1*H*-indol-3-yl)propyl]-1,3,4-oxadiazol-2-yl}sulfanyl)butanamide. A similar methodology was implemented for the structural characterization of the other derivatives in the synthesized series.

### 3.2 Urease inhibition and structure–activity relationship

The synthesized bi-heterocyclic butanamides, **8a–j**, were screened against urease of *Canavalia ensiformis* (Jack bean) and were found to have potent inhibitory potential against this enzyme, as was evident from their low $IC_{50}$ (μM) values (Table 1), relative to the standard, thiourea, which has an $IC_{50}$ value of 4.7455 ± 0.0546 μM. The jack bean urease was used only as a surrogate because the human urease is highly expensive and is not feasible for such *in vitro* investigations.[16–18]

Although the observed activity is the resultant of the whole molecule, a limited structure–activity relationship (SAR) was rationalized by analyzing the effect of different aryl moieties on the inhibitory potential. Fig. 5 displays the general structural features of the synthetic compounds.

Compound **8a** ($IC_{50}$ = 0.0523 ± 0.0044 μM) having a 4-ethyoxyphenyl ring showed a comparable activity with that of **8b** ($IC_{50}$ = 0.0542 ± 0.0211 μM) which bears a 2-ethylphenyl group. This indicates that the phenyl ring either having a 4-ethoxy or 2-ethyl group behaves almost similarly with the active site of the enzyme. However, compound **8c**, bearing an ethyl group at the 4-position of the phenyl ring, showed excellent inhibitory potential ($IC_{50}$ = 0.0175 ± 0.0065 μM) and was identified as the most active among all the synthetic analogues. This may be due to an appropriate interaction of the 4-ethylphenyl ring with the active site of enzyme (Fig. 6).

Among the three regio-isomers, **8d**, **8e** and **8f**, the molecule **8e**, bearing a 3-methylphenyl group, exhibited better inhibitory potential ($IC_{50}$ = 0.0323 ± 0.0119 μM), although, **8d** with a 2-methylphenyl moiety, also possessed very similar activity ($IC_{50}$ = 0.0717 ± 0.0152 μM). A minute reducing trend in activity was observed in **8f** which had the same methyl group at the 4-position of the phenyl ring ($IC_{50}$ = 0.1017 ± 0.0299 μM), which means that more efficient interactions are made with the enzyme when a methyl group is present at the *meta* position instead of the *ortho* or *para* position (Fig. 7).

Among the di-substituted molecules, compound **8h** and **8j**, having di-*ortho* substitutions, were found to be more suitable than the other analogues, and exhibited similar $IC_{50}$ values: 0.0251 ± 0.0083 and 0.0375 ± 0.0058 μM, respectively, although a methyl group at the 2-position in **8h** was replaced with an ethyl group in **8j**. The compound, **8h**, was the second most active compound of the series. In other two, di-methylated regio-isomers, **8g** and **8i**, the presence of two methyl groups at 3 and 5-positions of the phenyl ring in **8i** attributed this

 

Table 1 Urease inhibitory and hemolytic activity of bi-heterocyclic butanamides, **8a–j**[a]

| Compounds | Aryl part | Urease activity $IC_{50} \pm SEM$ (μM) | Hemolysis (%) (Mean ± SEM) |
|---|---|---|---|
| **8a** | 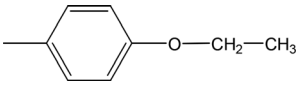 | 0.0523 ± 0.0044 | 3.16 ± 0.05 |
| **8b** | 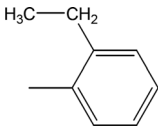 | 0.0542 ± 0.0211 | 2.41 ± 0.03 |
| **8c** | 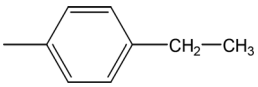 | 0.0175 ± 0.0065 | 0.62 ± 0.02 |
| **8d** | 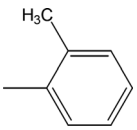 | 0.0717 ± 0.0152 | 5.18 ± 0.03 |
| **8e** | 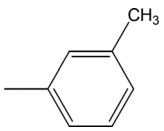 | 0.0323 ± 0.0119 | 5.92 ± 0.02 |
| **8f** | 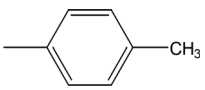 | 0.1017 ± 0.0299 | 3.51 ± 0.04 |
| **8g** | 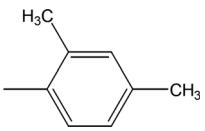 | 0.2002 ± 0.0122 | 1.41 ± 0.01 |
| **8h** | 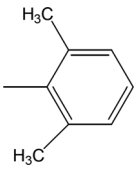 | 0.0251 ± 0.0083 | 2.63 ± 0.02 |
| **8i** | 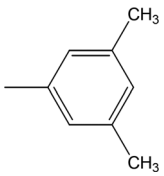 | 0.1244 ± 0.0318 | 7.32 ± 0.03 |
| **8j** | 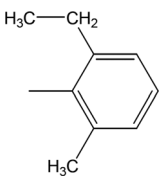 | 0.0375 ± 0.0058 | 9.63 ± 0.05 |
| Thiourea | | 4.7455 ± 0.0546 | — |
| Triton X | | — | 89.11 ± 0.01 |

[a] SEM = Standard error of the mean; values are expressed in mean ± SEM. PBS Hemolysis = 2.93 ± 0.01%.

molecule with slightly better inhibitory potential ($IC_{50}$ = 0.1244 ± 0.0318 μM) as compared to **8g** ($IC_{50}$ = 0.2002 ± 0.0122 μM) in which the two methyl groups were present at the 2- and 4-positions of the phenyl ring (Fig. 8).

### 3.3 Kinetic analysis

Based on our results, we selected the most potent compound **8c** to determine their inhibition type and inhibition constant on jack bean urease. The potential of these compounds to inhibit

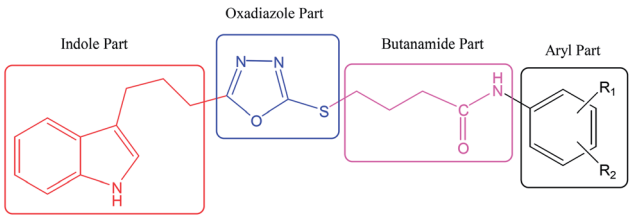


Fig. 5 General structural features of compounds **8a–j**.

the free enzyme and enzyme substrate complex was determined in terms of the EI and ESI constants respectively. The kinetic studies of the enzyme by the Lineweaver–Burk plot of $1/V$ *versus* 1/[S] in the presence of different compound concentrations gave a series of straight lines (Fig. 9A). The results of compound **8c** showed that the compound intersected within the second quadrant. The analysis showed that $V_{max}$ decreased with the increase in inhibitor dosage, while $K_m$ remained the same. This behavior indicated that compound **8c** inhibited the urease non-competitively to form an enzyme inhibitor complex. The secondary plot of slope against the concentration of inhibitors showed the enzyme-inhibitor dissociation constant ($K_i$) (Fig. 9B).

The kinetic results are presented in the Table 2.

### 3.4 Structural and physiochemical assessment of jack bean urease

Jack bean urease is a class of hydrolase protein containing couple of nickel atoms in the active region of target protein. The VADAR analysis justified that the Jack bean urease architecture consists of 27% α-helices, 31% β-sheets and 41% coils. Moreover, Ramachandran plots also indicated that 97.5% of the residues were present in the favored regions, which shows good precision of phi ($\varphi$) and psi ($\psi$) angles among the coordinates of the jack bean urease structure (Fig. S1†).

**3.4.1 Molecular docking binding energy analysis.** The ligand-protein docked complexes were analyzed on the basis of the minimum energy values and ligand conformational interactions pattern. The generated results showed that all the compounds (**8a–j**) displayed good docking energy values (kcal $mol^{-1}$) and bind in the binding pocket of urease (Table 3). In all the docking complexes the predicted energy values were similar and no marked energy value difference was observed amongst all the docking structures. Prior research show that the standard error for Autodock is 2.5 kcal $mol^{-1}$ (http://autodock.scripps.edu/). Therefore, to prioritize one ligand over others, it must have higher than a 2.5 kcal $mol^{-1}$ energy value difference compared to other ligands. In all the docking complexes, the predicted energy values difference was less than the standard error energy value. This result was obtained because the basic nucleus of all the synthesized compounds was similar and most of the ligands possess similar and efficient binding affinity values with no significant energy fluctuations. The comparative docking analysis and inhibition potential justified that **8c** has good therapeutic potential compared to all other compounds.

**3.4.2 Binding pocket analysis.** The binding pocket analysis showed that all the synthesized ligands (**8a–j**) were narrowed in the binding pocket of the target protein close to the nickel ions. All the docked structures were superimposed to check the binding configurations of all the ligands within the active region of the target protein. The results show that all the synthesized ligands were bound at same positioned residues with different conformational poses in binding pocket. The binding of all the ligands at same position also justify our docking reliability and predicted results (Fig. 10A). Based on *in vitro* analysis, **8c** showed good enzyme inhibition potential therefore, ligand **8c** was selected to keenly observe the binding interaction pattern. The **8c**-docking complex showed that the indole moiety showed its penetration toward nickel metal. The substituted functional moiety showed good conformation position inside the active region of the target protein (Fig. 10B).

**3.4.3 Binding analyses of synthesized compounds against jack bean urease.** The ligands-protein binding analyses showed that **8c** was confined in the active binding pocket of the target protein. The **8c**-docked complex revealed a good conformational state with hydrogen bond and hydrophobic interactions within the receptor binding pocket. The docking results of **8c**–

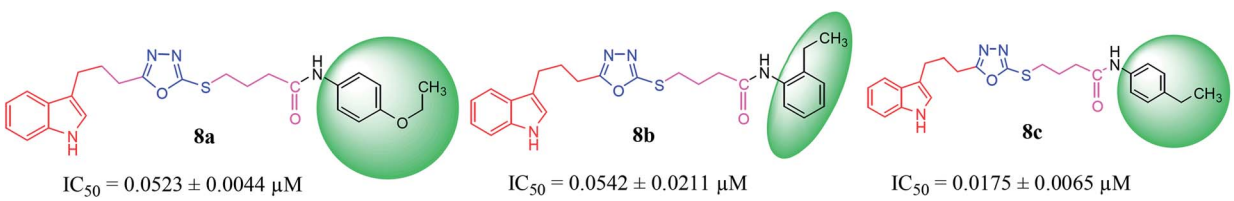


Fig. 6 Structure–activity relationship of compounds **8a**, **8b**, and **8c**.

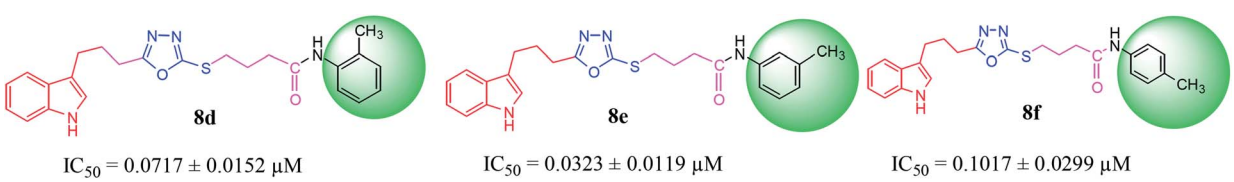


Fig. 7 Structure–activity relationship of compounds **8d**, **8e**, and **8f**.

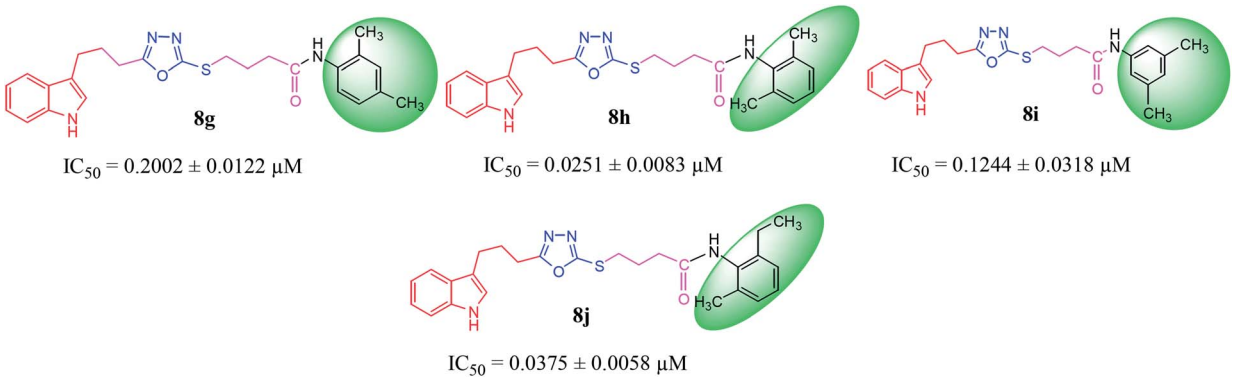


Fig. 8 Structure–activity relationship of compounds **8g**, **8h**, **8i**, and **8j**.

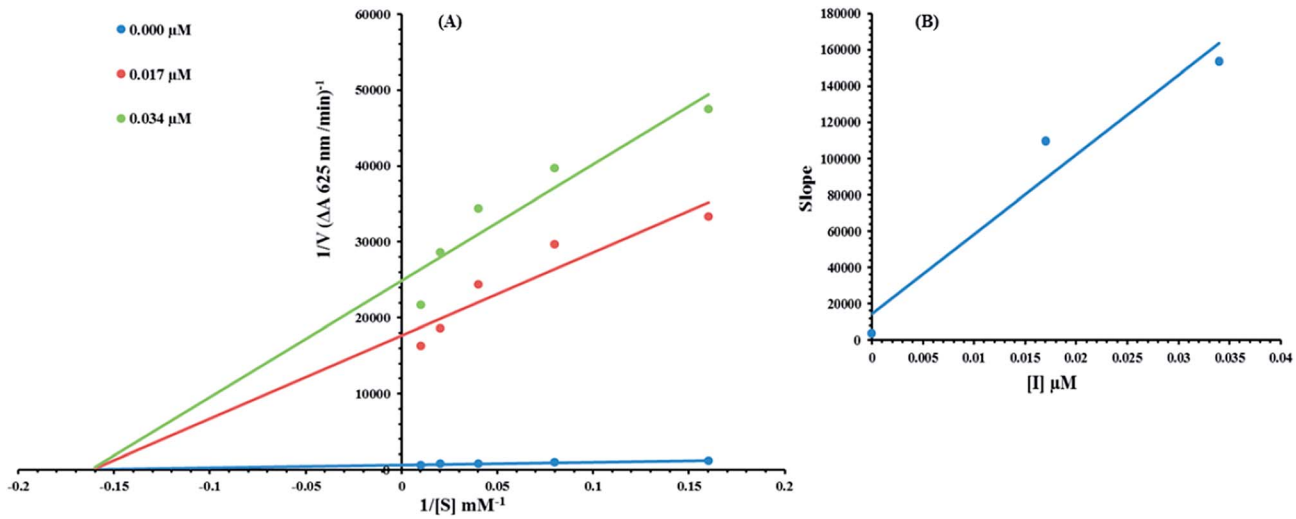


Fig. 9 Lineweaver–Burk plots for inhibition of urease in the presence of compound **8c**. (A) Concentrations of **8c** were 0.00, 0.017 and 0.034 μM. (B) The insets represent the plot of the slope or the vertical *versus* inhibitor **8c** concentrations to determine inhibition constants. The lines were drawn using linear least squares fit.

receptor complex showed that two hydrogen and a single hydrophobic interaction were observed at Asp494, Arg439 and His593 residues, respectively. The nitrogen of the oxadiazol ring formed a strong hydrogen bond with Arg439 with a bond distance of 2.96 Å. Similarly, the nitrogen of the indole ring also formed a hydrogen bond with Asp494 with a bond length of 2.96 Å. Both amino acids are key residues in the active binding pocket site. Our ligand **8c** showed good attachment inside the active region of the target structure with good hydrogen bonding distances. Moreover, another π–π interaction was observed between the indole ring and the aromatic His593 residue with a bond distance of 5.01 Å. The binding interaction pattern within the binding pocket and against the interacted residues is mentioned in Fig. 11A and B. The 2D graphical depiction of all the other docking complexes is mentioned in the ESI (Fig. S2–S10†). Literature reports also favor our docking

Table 2 Kinetic parameters of the jack bean urease for urea activity in the presence of different concentrations of **8c**[a]

| Concentration (μM) | $V_{max}$ (Δ*A*/Min) | $K_m$ (mM) | Inhibition type | $K_i$ (μM) |
|---|---|---|---|---|
| 0.00 | 0.001724017 | 5.9 | Non-competitive | 0.003 |
| 0.017 | $6.11923 \times 10^{-5}$ | 5.9 | | |
| 0.034 | $4.59941 \times 10^{-5}$ | 5.9 | | |

[a] $V_{max}$ is the reaction velocity, $K_m$ is the Michaelis–Menten constant, $K_i$ is the EI dissociation constant.

Table 3 Docking results of synthesized compounds

| Docking complexes | Binding affinity (kcal mol$^{-1}$) |
|---|---|
| **8a** | −8.3 |
| **8b** | −8.4 |
| **8c** | −8.4 |
| **8d** | −8.5 |
| **8e** | −8.6 |
| **8f** | −9.5 |
| **8g** | −8.6 |
| **8h** | −9.4 |
| **8i** | −8.5 |
| **8j** | −9.1 |

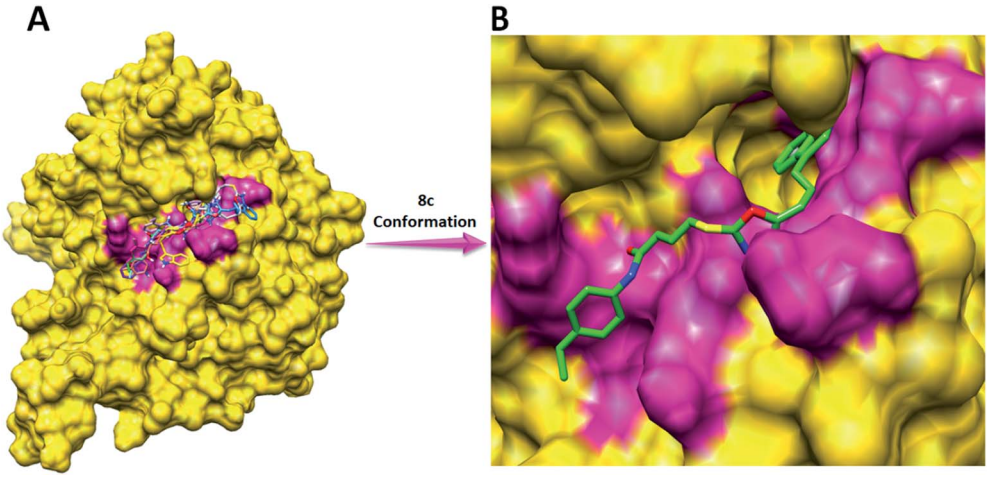


Fig. 10 Binding pocket analysis of the ligands. (A) Superimposed docked structures (B) binding conformation of **8c** within the binding pocket.

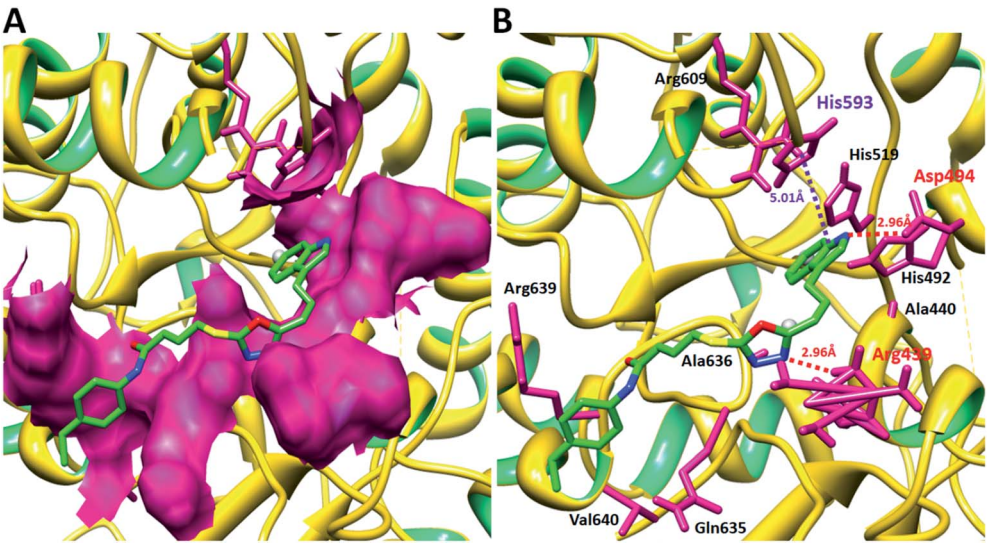


Fig. 11 Docking interaction **8c** with receptor molecule. (A) The protein binding pocket in the surface format is represented in pink, while the protein structure is highlighted in yellow in ribbon format. (B) The **8c**-docking complex ligand structure is represented in green, while their functional groups such as oxygen, nitrogen and sulphur are shown in red, blue and yellow, respectively. Amino acids are highlighted in light pink, and red and purple dotted lines represent hydrogen and hydrophobic binding with the distance mentioned in angstrom (Å). Nickel metal is represented as grey circles.

results which strengthen our discussions on the ligand binding and conformational position within the active region of the target protein.[25–30]

### 3.5 Hemolytic activity

All the as-synthesized bi-heterocyclic butamides, **8a–j**, were also subjected to hemolytic assay to find out their cytotoxicity profile. The results of the percentage hemolysis (%) are shown in Table 1. Our results showed that all the compounds of this series have moderate toxicity towards red blood cell membrane. Maximum membrane toxicity was shown by the compound **8j** (9.63 ± 0.05%) which is feeble relative to the positive control, Triton X having hemolysis of 89.11 ± 0.01%. The minimum toxicity was pragmatic in **8c** (0.62 ± 0.02%). Precisely, a very low toxicity was also observed for molecules **8g** (1.41 ± 0.01%), **8b** (2.41 ± 0.03%) and **8h** (2.63 ± 0.02%) respectively, relative to that of Triton-X.

## 4. Conclusion

The targeted 2-({5-[3-(1*H*-indol-3-yl)propyl]-1,3,4-oxadiazol-2-yl}sulfanyl)-*N*-(substituted-phenyl)butanamides (**8a–j**) were synthesized in good yields and these molecules, owing to their unique skeleton, possessed potent inhibitory potential against urease. The molecular docking results were in complete agreement with enzyme inhibition data. These molecules were screened for their *in vitro* inhibitory potential against urease enzyme and were found to be potent inhibitors. The enzyme inhibitory potential (0.0175 ± 0.0065) and kinetics results showed that compound **8c** inhibited the enzyme competitively

 

with $K_i$ value 0.003 μM. The *in silico* study of these scaffolds was in full agreement with the experimental data and **8c** showed good interaction within the active region of the target protein, having a good binding energy value ($-8.4$ kcal mol$^{-1}$). Almost all the molecules also demonstrated low cytotoxicity. Therefore, these studies conclude that the newly synthesized molecules might serve as promising drug candidates for further structural optimizations and drug designing studies.

## Conflicts of interest

There are no conflicts to declare.

## Acknowledgements

The authors acknowledge the Higher Education Commission (HEC) of Pakistan for financial support regarding EI-MS analysis.

## References

1 P. Hardik, D. Nilesh, P. Jagath and P. Bhagirath, *Int. J. Drug Res. Technol.*, 2012, **2**(3), 225–230.
2 S. Agarwal, S. Cammerer, S. Filali, W. Frohner, J. Knoll and M. P. Krahl, *Curr. Org. Chem.*, 2005, **9**, 1601–1614.
3 J. Hajicek, *Czech. Chem. Commun.*, 2007, **72**, 821–898.
4 M. A. Metwally, S. Shaaban, B. F. Abdel-Wahab and G. A. El-Hiti, *Curr. Org. Chem.*, 2009, **13**, 1475–1496.
5 M. S. Chande, K. A. Puthamane, P. A. Brave, R. R. Khanwelkar and D. S. Venkatraman, *J. Braz. Chem. Soc.*, 2008, **19**(1), 42–52.
6 M. Yar, M. Bajda, R. A. Mehmood, L. R. Sidra, N. Ullah, L. Shahzadi, M. Ashraf, T. Ismail, S. A. Shahzad, Z. A. Khan, S. A. R. Naqvi and N. Mahmood, *Lett. Drug Des. Discovery*, 2014, **11**, 331–338.
7 M. Amir and S. Shahani, *Indian J. Heterocycl. Chem.*, 1998, **8**, 107–110.
8 J. Hazarika and J. C. S. Kataky, *Indian J. Heterocycl. Chem.*, 1998, **7**, 83–92.
9 B. S. Holla, C. S. Prasanna, B. Poojary, K. S. Rao, K. Shridhara and U. G. Bhat, *Indian J. Chem.*, 2004, **43B**, 864–868.
10 M. I. Choudhary, *US pat.* 20150368214 A1, 2015.
11 M. A. Lodhi, J. Hussain, M. A. Abbasi, A. R. Jassbi, M. I. Choudhary and V. U. Ahmad, *J. Enzyme Inhib. Med. Chem.*, 2006, **21**(5), 531–535.
12 K. Rubab, M. A. Abbasi, Aziz-ur-Rehman, S. Z. Siddiqui and M. N. Akhtar, *Trop. J. Pharm. Res.*, 2016a, **15**(7), 1515–1524.
13 K. Rubab, M. A. Abbasi, Aziz-ur-Rehman, S. Z. Siddiqui, M. Ashraf and A. Shaukat, *Trop. J. Pharm. Res.*, 2016b, **15**(7), 1525–1533.
14 M. A. Abbasi, M. Hassan, Aziz-ur-Rehman, S. Z. Siddiqui, H. Raza, S. A. A. Shah and S.-Y. Seo, *Bioorg. Med. Chem.*, 2018, **26**, 3791–3804.
15 M. W. Weatherburn, *Anal. Chem.*, 1967, **39**(8), 971–974.
16 H. Raza, Q. Abbas, M. Hassan, S.-H. Eo, Z. Ashraf, D. Kim, A. R. Phull, S. J. Kim, S. K. Kang and S.-Y. Seo, *Pharm. Biol.*, 2017, **55**(1), 218–226.
17 P. A. Channar, A. Saeed, F. Albericio, F. A. Larik, Q. Abbas, M. Hassan, H. Raza and S.-Y. Seo, *Molecules*, 2017, **22**(8), 1352–XXXC.
18 A. Saeed, F. A. Larik, P. A. Channar, H. Mehfooz, M. H. Ashraf, Q. Abbas, M. Hassan and S.-Y. Seo, *Chem. Biol. Drug Des.*, 2017, **90**, 764–777.
19 E. F. Pettersen, T. D. Goddard, C. C. Huang, G. S. Couch, D. M. Greenblatt, E. C. Meng and T. E. Ferrin, *J. Comput. Chem.*, 2004, **25**, 1605–1612.
20 L. Willard, A. Ranjan, H. Zhang, H. Monzavi, R. F. Boyko, B. D. Sykes and D. S. Wishart, *Nucleic Acids Res.*, 2003, **31**, 3316–3319.
21 S. Dallakyan and A. J. Olson, *Methods Mol. Biol.*, 2015, **1263**, 243–250.
22 Studio D., Discovery,*version 2.1. Accelrys*,San Diego, CA,2008.
23 M. Shahid, S. A. Bukhari, Y. Gul, H. Munir, F. Anjum, M. Zuber, T. Jamil and K. M. Zia, *Int. J. Biol. Macromol.*, 2013, **62**, 172–179.
24 C. R. Yang, Y. Zhang, M. R. Jacob, S. I. Khan, Y. J. Yhang and X. C. Li, *Antimicrob. Agents Chemother.*, 2006, **50**(5), 1710–1714.
25 T. Abdul-Fattah, A. Saeed, P. A. Channar, Z. Ashraf, Q. Abbas, M. Hassan and F. A. Larik, *Chem. Biol. Drug Des.*, 2018, **91**, 434–447.
26 P. A. Channar, A. Saeed, F. Albericio, F. A. Larik, Q. Abbas, M. Hassan, H. Raza and S. Y. Seo, *Molecules*, 2017, **22**, E1352.
27 A. Saeed, S. Ur-Rehman, P. A. Channar, F. A. Larik, Q. Abbas, M. Hassan, H. Raza and S. Y. Seo, *Drug Res.*, 2017, **67**, 596–605.
28 A. Saeed, P. A. Mahesar, P. A. Channar, F. A. Larik, Q. Abbas, M. Hassan, H. Raza and S. Y. Seo, *Chem. Biodiversity*, 2017, **14**, e1700035.
29 A. Saeed, S. Rehman, P. A. Channar, F. A. Larik, Q. Abbas, M. Hassan, H. Raza, U. Flörke and S. Y. Seo, *J. Taiwan Inst. Chem. Eng.*, 2017, **77**, 54–63.
30 A. Saeed, F. A. Larik, P. A. Channar, H. Mehfooz, M. H. Ashraf, Q. Abbas, M. Hassan and S. Y. Seo, *Chem. Biol. Drug Des.*, 2017, **90**, 764–777.